Government of **Western Australia**
Department of **Mines and Petroleum**

RECORD 2016/14

MINERALOGY OF GOLD FROM THE PAULSENS AND MOUNT OLYMPUS DEPOSITS, NORTHERN CAPRICORN OROGEN, WESTERN AUSTRALIA

by
EA Hancock and AM Thorne

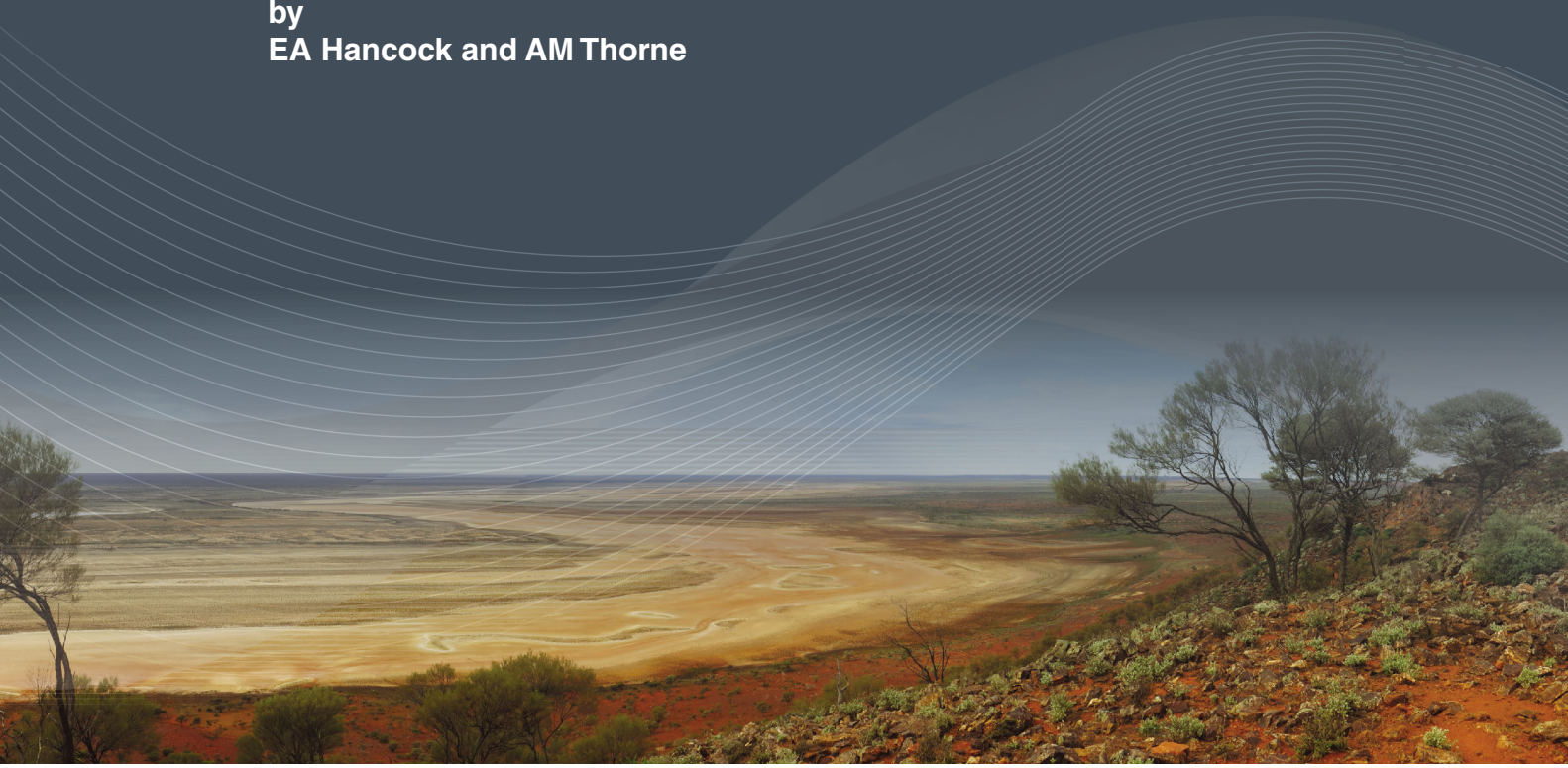

Geological Survey of Western Australia

Government of **Western Australia**
Department of **Mines and Petroleum**

Record 2016/14

MINERALOGY OF GOLD FROM THE PAULSENS AND MOUNT OLYMPUS DEPOSITS, NORTHERN CAPRICORN OROGEN, WESTERN AUSTRALIA

by
EA Hancock and AM Thorne

Perth 2016

Geological Survey of Western Australia

MINISTER FOR MINES AND PETROLEUM
Hon. Sean K L'Estrange MLA

ACTING DIRECTOR GENERAL, DEPARTMENT OF MINES AND PETROLEUM
Tim Griffin

EXECUTIVE DIRECTOR, GEOLOGICAL SURVEY OF WESTERN AUSTRALIA
Rick Rogerson

REFERENCE
The recommended reference for this publication is:
Hancock, EA and Thorne, AM 2016, Mineralogy of gold from the Paulsens and Mount Olympus deposits, northern Capricorn Orogen, Western Australia: Geological Survey of Western Australia, Record 2016/14, 16p.

National Library of Australia Card Number and ISBN 978-1-74168-711-8

Grid references in this publication refer to the Geocentric Datum of Australia 1994 (GDA94). Locations mentioned in the text are referenced using Map Grid Australia (MGA) coordinates, Zone 51. All locations are quoted to at least the nearest 100 m.

Published 2016 by Geological Survey of Western Australia
This Record is published in digital format (PDF) and is available online at <www.dmp.wa.gov.au/GSWApublications>.

Further details of geological products and maps produced by the Geological Survey of Western Australia are available from:
Information Centre
Department of Mines and Petroleum
100 Plain Street
EAST PERTH WESTERN AUSTRALIA 6004
Telephone: +61 8 9222 3459 Facsimile: +61 8 9222 3444
www.dmp.wa.gov.au/GSWApublications

Cover image: Elongate salt lake on the Yilgarn Craton — part of the Moore–Monger paleovalley — here viewed from the top of Wownaminya Hill, 20 km southeast of Yalgoo, Murchison Goldfields. Photograph taken by I Zibra for the Geological Survey of Western Australia

Contents

Figures

Tables

Mineralogy of gold from the Paulsens and Mount Olympus deposits, northern Capricorn Orogen, Western Australia

by

EA Hancock and AM Thorne

Abstract

The mineralogy of quartz vein-hosted lode gold from Paulsens Mine and placer gold from the Mount Olympus area in the northern Capricorn Orogen was examined to better understand the physical and chemical conditions and relative timing of gold mineralization. Although there are differences in host-rock geology, both the Paulsens and Mount Olympus deposits are located close to the Nanjilgardy Fault, a major, mantle-tapping structure, formed along the southern margin of the exposed Pilbara Craton.

Previous studies show that gold at Paulsens is found in three settings within the quartz vein host rock: 1) a very fine-grained mode that is spatially associated with massive pyrite; 2) along stylolites, especially in the Lower Zone; and 3) less commonly, a coarse-grained mode in vein quartz. The results from our study show that gold is also spatially associated with massive pyrrhotite within the quartz vein host. Only visible gold associated with fractures and stylolites, and fine-grained gold spatially associated with massive sulfide, was made available for this study. It occurs in six assemblages: 1) irregular fracture-fill gold in stylolitic quartz. Gold grains are >100 µm and have an Ag content of 6.8 – 7.6 wt% and elevated levels of Cu, Sb, and Hg. They display a simple polycrystalline microstructure; 2) interstitial gold in arsenopyrite crystals. Gold grains are small (< 500 µm) with a polycrystalline twinned microstructure and contain 7 wt% Ag; 3) spongy-textured gold in pyrite within arsenopyrite. Gold is very fine-grained and dust like (≤20 µm); 4) isometric and drop-like gold in massive pyrrhotite. Gold grains range in size from 10–600 µm and display a simple mono- and polycrystalline twinned microstructure. They contain 8.0 – 8.5 wt% of Ag and show a general enrichment in Cu, Sb, and Hg and an occasional enrichment in Co, Ni, and Bi; 5) irregular gold grains in cavities of massive pyrrhotite. Gold grains are small (10–100 µm) and contain 6 wt% Ag, together with high concentrations of Cu, Sb, and Hg. The internal structure of gold grains appears to be monocrystalline; 6) irregular gold grains within pyrrhotite that replaces massive pyrite. Gold grains range in size from 10–200 µm and shapes are irregular and sometimes angular. They contain 6.6 – 7.2 wt% Ag and high levels of Cu, Sb, and Hg with occasional enrichment in Co, Ni, and Bi. The gold has a simple monocrystalline microstructure with some twin planes.

Placer gold nuggets from Mount Olympus were derived from ferruginous quartz veins, located 2–3 km from the main sediment-hosted mineralization, which has been dated at c. 1738 Ma. The placer gold shows considerable variation in its morphology and the amount of quartz and Fe-oxide inclusions. All gold has a primary polycrystalline and twinned microstructure, with only minor deformed, incoherent, broken and curved twin planes and translated zones. Thin, high-purity intergranular veinlets are abundant. The placer gold has an Ag content ranging from <3.8 to 9.9 wt%. Using LA-ICP-MS analysis, only four elements (Ag, Cu, Sb, and Hg) are present in concentration levels higher than background. The relative content of these elements, especially Sb, is variable, and all samples have high values of Hg.

The majority of gold from Paulsens (assemblages 1, 2, 5, and 6) and quartz vein-sourced placer gold from Mount Olympus show similarities in their primary microstructure and chemistry that indicate both were precipitated from low-temperature hydrothermal solutions under physically dynamic, but chemically stable conditions. Gold from both sources experienced only weak, low-pressure and low-temperature postdepositional alteration, although in the case of the placer gold the primary features have been modified in response to supergene processes. The depositional setting for the sulfide-hosted gold in Paulsens assemblages 3 and 4 is uncertain, but appears to have occurred during an earlier, relatively low-temperature hydrothermal melting event or events.

Evidence presented here suggests that most of the gold mineralization at Paulsens (assemblages 1, 2, 5, and 6) and in Mount Olympus vein quartz post-dates both the 2215–2145 Ma Ophthalmian Orogeny and the 1820–1776 Ma Capricorn Orogeny. It might have occurred during the final stages of c.1738 Ma dextral strike-slip faulting in the southern Pilbara, but could also have formed during one of the many Paleoproterozoic to Neoproterozoic tectonic events recorded in the central Capricorn Orogen. The ages of the two older gold mineralizing events at Paulsens (assemblages 3 and 4) are also unknown and could have occurred at any time between the initial deformation of the host stratigraphy (Ophthalmian Orogeny?) and the formation of Paulsens assemblages 1, 2, 5, and 6.

KEYWORDS: gold minerals, gold placer deposits, lode deposits

Introduction

The principal aim of this study is to investigate the mineralogy of lode and placer gold from the Paulsens and Mount Olympus deposits, in order to better understand the physical and chemical conditions during gold mineralization. It is based upon the premise that the microstructural and trace-element features of gold grains preserve information on the relative timing and chemical environment of primary (hypogene) formation and any subsequent physical or chemical, hydrothermal or supergene reworking (Petrovskaya, 1973; Nikolaeva et al., 2004). A caveat in this particular study is that the conclusions drawn are based on a limited number of samples.

Geological setting

The Paulsens and Mount Olympus gold deposits are located in the northern part of the Capricorn Orogen (Fig. 1), close to splays associated with the Nanjilgardy Fault system, which recent seismic reflection profiling shows to be a major, mantle-tapping structure formed along the southern margin of the exposed Pilbara Craton (Thorne et al., 2011; Johnson et al., 2013).

The Paulsens gold deposit occurs in the northwestern part of Wyloo Dome, which is interpreted to have formed during the 2215–2145 Ma Ophthalmian Orogeny (Rasmussen et al., 2005), and to have been subsequently reactivated during the 1820–1770 Ma Capricorn Orogeny (Sheppard et al., 2005) and c. 1738 Ma dextral strike-slip faulting (Sener et al., 2005). Gold mineralization is contained in a 40 m thick quartz vein, mostly at its hanging wall and footwall contacts (the Upper and Lower Zones, respectively) with surrounding greenschist facies Archean metasedimentary and metavolcanic rocks of the upper Hardey Formation, Fortescue Group, and a younger gabbro dyke referred to as the Paulsen's Gabbro. This dyke is shallow dipping, oriented at a low angle to bedding, and locally foliated by two or more ductile fabrics (Fig. 2; Northern Star Resources Ltd, 2012).

Gold occurs in four styles: 1) a very fine-grained phase spatially associated with massive pyrite, especially in the Upper Zone; 2) along stylolites, especially in the Lower Zone; 3) a less-common, coarse-grained phase in vein quartz (Northern Star Resources Ltd, 2012); and 4) spatially associated with massive pyrrhotite within the quartz vein host (this study).

The Mount Olympus gold deposit lies in the Ashburton Basin, to the southeast of Bellary Dome near Paraburdoo (Fig. 1). Mineralization comprises submicroscopic gold inclusions in disseminated arsenian pyrite, associated with quartz–sericite alteration, in Paleoproterozoic rocks of the Wyloo and Shingle Creek Groups (Thorne, 2016a,b) and Wooly Dolomite (Krapež et al., 2015). The mineralization has an age of c. 1738 Ma, based on in situ U–Pb SHRIMP dating of hydrothermal xenotime (Sener et al., 2005). It post-dates the regional metamorphism, and Young et al. (2003) link it temporally and spatially with a major period of dextral strike-slip faulting that corresponds to the D_{2ash} event described by Thorne et al. (2011).

Methodology

Sampling

Paulsens

Six samples of vein-hosted gold from Paulsens Gold Mine were analysed. Their locations and material types are summarized in Table 1. Two of these samples are from core drilled through massive sulfide in the Voyager 1 extension of the Upper Zone (Fig. 3). The other four samples are of gold-bearing stylolitic quartz vein material obtained from the underground workings (Fig. 4) in both Upper and Lower Zones. Stylolitic quartz veins with coarse gold are abundant for the Lower Zone (e.g. GSWA sample 201915) and they are not typical for the Upper Zone, where gold-bearing massive sulfides are predominant (e.g. GSWA samples 201916 and 201917). Visible gold is rarely seen in graphitic stylolites in the Upper Zone, such as in samples 201909–201911.

Mount Olympus

Seven small nuggets of placer gold from the Mount Olympus area were donated to the Geological Survey of Western Australia (GSWA) by prospectors working on the Mount Olympus tenement (Fig. 5 and Table 1). Two of these nuggets were collected from proximal, quartz-rich colluvium, overlying faulted Beasley River Quartzite 3.2 km west-northwest of the main Mount Olympus workings (GSWA sample 201912, numbers 1 and 2). A single nugget was obtained from proximal colluvium overlying faulted Mount McGrath Formation 2.7 km east-southeast of the main Mount Olympus workings (GSWA sample 201913). The remaining four nuggets were collected from proximal colluvium overlying Cheela Springs Basalt, 2.7 km east of the main Mount Olympus workings (GSWA sample 201914, numbers 1, 2, 3 and 4).

Mineralogical analyses

The mineralogical methodologies used in this Report are based on those described by Hancock and Thorne (2011). All gold-bearing samples were first described and photographed. Stylolite mineralogy in GSWA samples 201909 and 201910 was studied by rapid reflectance infrared spectroscopy using the GSWA HyLogger-3 facility. Three stylolite samples from the Upper Zone with large visible gold grains were crushed and the gold extracted by hand. The gold was then mounted in epoxy resin, cut and polished. Other samples contained smaller gold grains; hence, were initially prepared as polished thin sections. Ag content of the gold and identification of any associated minerals were determined using a field emission scanning electron microscope fitted with an energy dispersive X-ray spectroscope (FE-SEM/EDX). All gold grains were then etched with aqua regia, and their internal structure was analysed optically. The trace-element chemistry of selected features in the gold

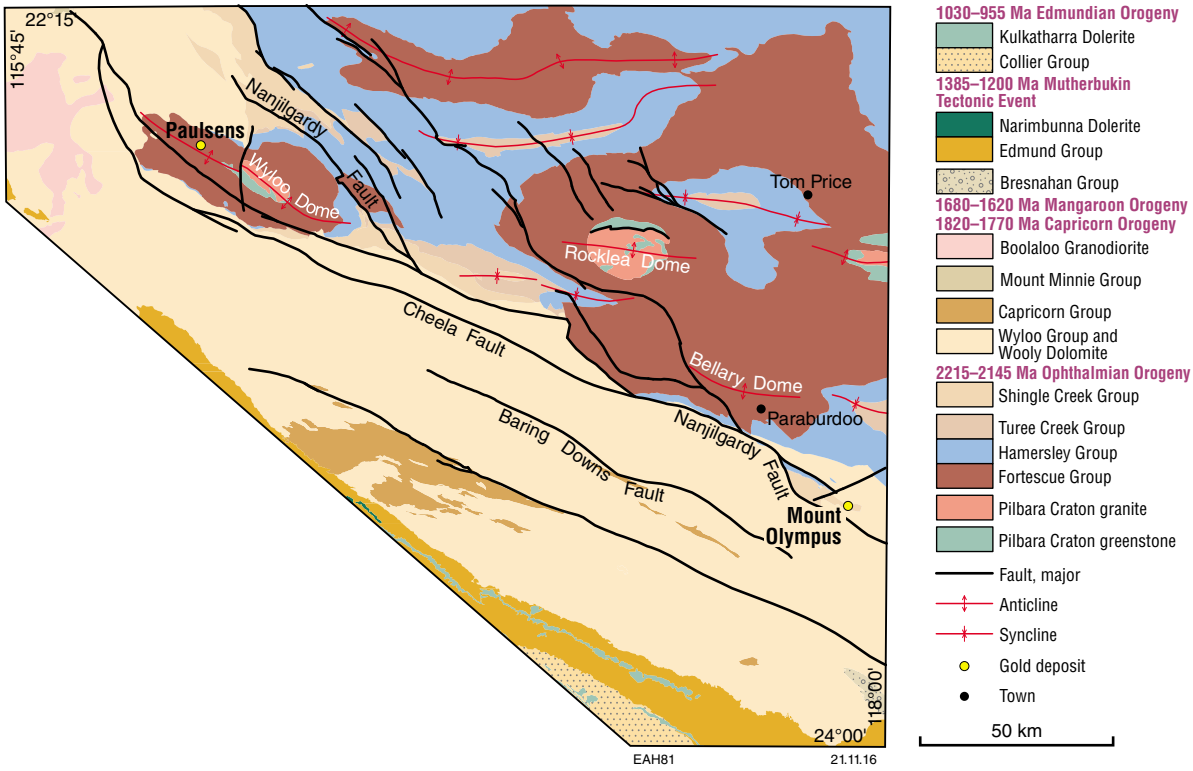

Figure 1. Geological map of the northern Capricorn Orogen showing the location of the Paulsens and Mount Olympus gold deposits

microstructure was then analysed using laser ablation inductively coupled plasma mass spectrometry (LA-ICP-MS).

FE-SEM/EDX analysis

The Ag content of the gold grains was measured using a Tescan MIRA 3 FE-SEM fitted with Oxford X-Max 50 EDS at CSIRO, Kensington, Western Australia. All samples were re-polished and coated with carbon prior to data acquisition and the results were calibrated using CSIRO gold standards.

LA-ICP-MS analysis

LA-ICP-MS analyses of 22 gold grains from all Paulsens and Mount Olympus samples were carried out at The University of Western Australia, using an Agilent 7500CS ICP-MS system. Instrumental settings were optimized using a NIST 610 glass standard, and Gold AUSTD1 standard. Samples were ablated for 30 seconds at 10 Hz using a 213 nm New Wave UP213 laser ablation unit, creating a spot size of 50 µm (Watling et al., 1994). Due to nonhomogeneous matrix of gold standards, the resulting data are reported here as counts per second (cps).

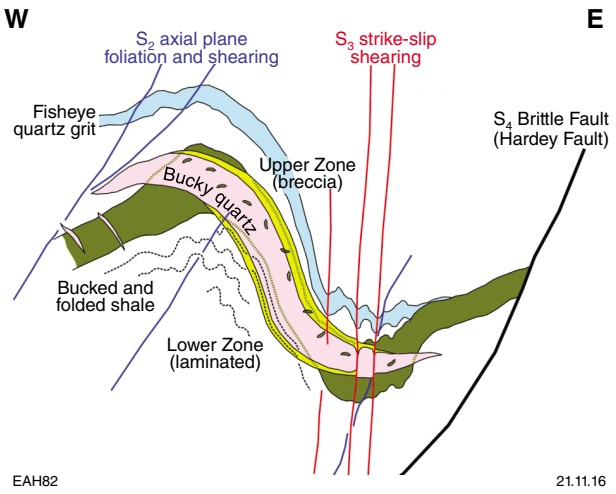

Figure 2. Schematic cross-section of the Paulsens deposit depicting the major structural and lithological components. Upper and lower mineralized zones within the main quartz veins probably reflect the host rock where they developed. The Upper Zone (breccia/sulfide) has incorporated pieces of Paulsens Gabbro, while the Lower Zone (laminated) has incorporated ribbony clasts of graphitic shale. Image supplied by Northern Star Resources Ltd

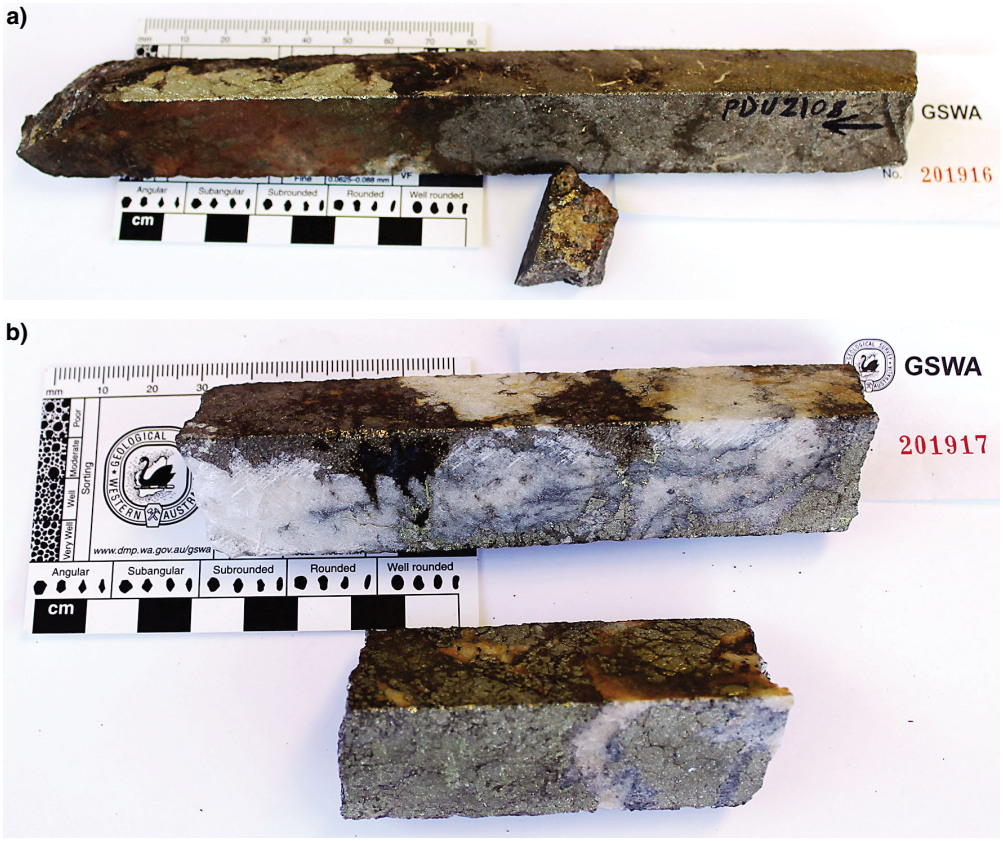

EAH83 19.09.16

Figure 3. **Two drillcore samples of gold-bearing massive sulfides from the Voyager 1 part of the Upper Zone at Paulsens: a) pyrite–pyrrhotite, GSWA 201916; b) quartz–pyrite, GSWA 201917**

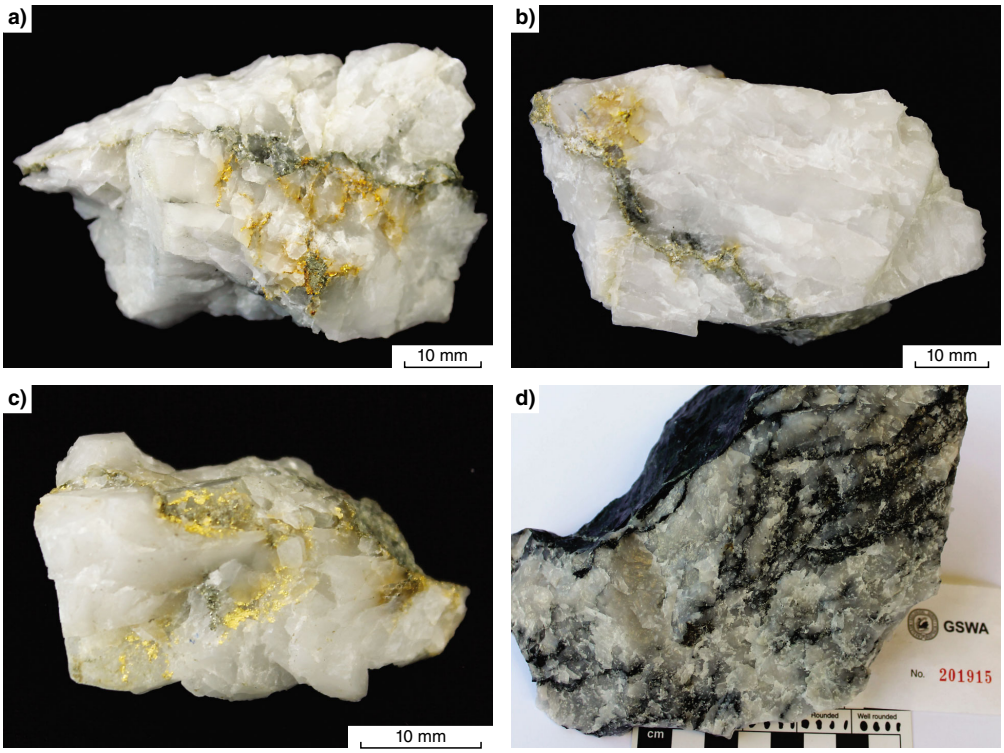

EAH84 06.09.16

Figure 4. **Four gold-bearing stylolitic quartz vein samples from Paulsens: a) GSWA 201909, Voyager 1, Upper Zone; b) GSWA 201910, Voyager 1, Upper Zone; c) GSWA 201911, Voyager 1, Upper Zone; d) GSWA 201915, Lower Zone**

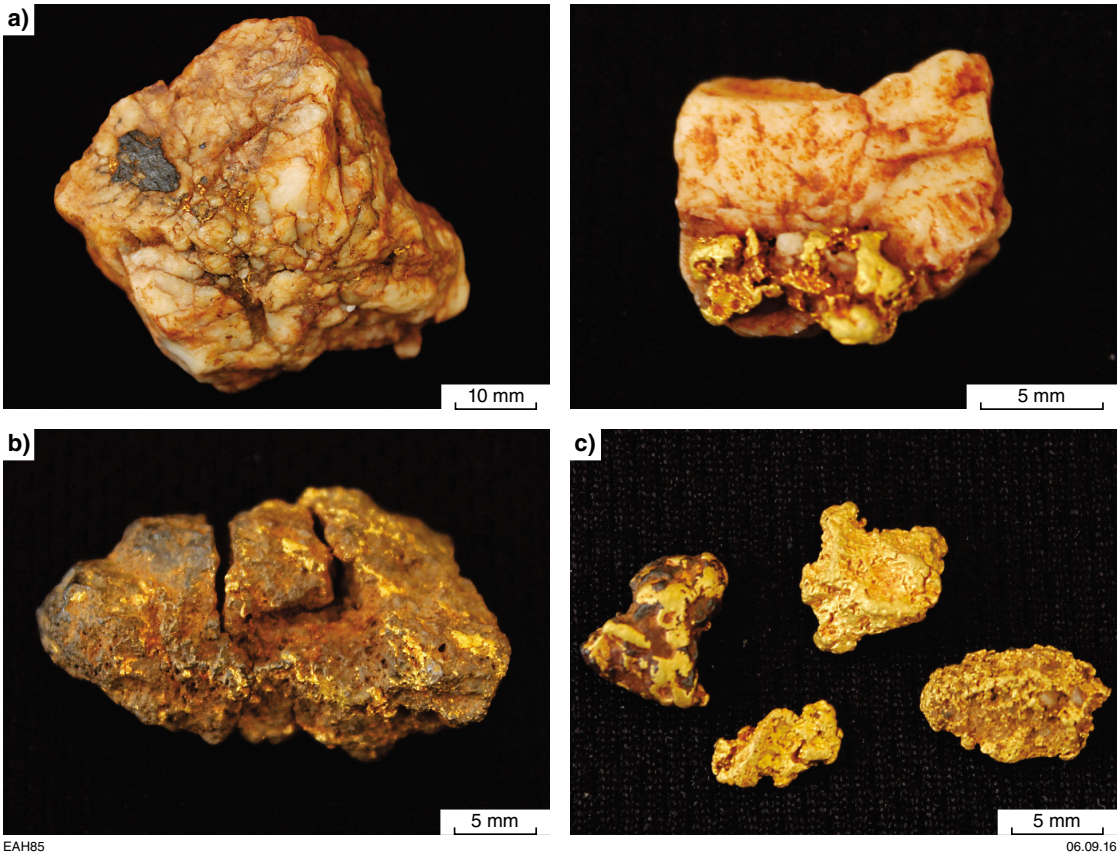

Figure 5. Seven samples of placer gold from the Mount Olympus area: a) GSWA 201912 comprises two examples of gold-bearing vein quartz; b) GSWA 201913 is a single ferruginous gold nugget; c) GSWA 201914 is composed of four gold nuggets, each containing variable amounts of iron oxides

Table 1. Sample locations

GSWA sample no.	*Location*	*Material type*	*Easting*	*Northing*	*Depth RL*
	Paulsens				
201909	Upper Zone, Voyager 1	Gold-rich quartz vein specimen from underground workings	421750	7503839	420
201910	Upper Zone, Voyager 1	Gold-rich quartz vein specimen from underground workings	421750	7503839	420
201911	Upper Zone, Voyager 1	Gold-rich quartz vein specimen from underground workings	421750	7503839	420
201915	Lower Zone	Gold-rich quartz vein specimen from underground workings	422121	7503386	860
201916	Upper Zone, Voyager 1; drillhole PDU2108, 151.8 m	Drillcore with massive pyrrhotite and gold	421626	7503994	412
201917	Upper Zone, Voyager 1; drillhole PDU2112, 157.2 m	Drillcore with massive pyrite and gold	421626	7503995	412
	Mount Olympus				
201912	Colluvium	Two gold nuggets	589234	7409060	N/a
201913	Colluvium	Gold nugget	595163	7407447	N/a
201914	Colluvium	Four gold nuggets	594986	7408172	N/a

Discussion of element variation is therefore based on their relative concentrations, rather than in terms of absolute concentrations (e.g. ppm). Values less than 1000 cps are treated as background, following the work of Hancock et al. (2009). Fifty-seven elements between atomic mass 45 (scandium) and 238 (uranium) were analysed.

Trace elements in the gold microstructure occur as submicroscopic mineral inclusions and as limited solid solutions. In contrast, lithophile elements, e.g. Mg, Al, Fe, Ti, V, Mn, Ba, can be contaminants derived from the surrounding rocks during analyses of very small gold grains. They are distinguished from trace elements derived from micro-inclusions in gold by their consistently high concentrations in very small grains as opposed to their absence in larger grains. These lithophile elements are not discussed in this Record.

HyLogger analysis

The HyLogger-3 spectrometer scans in the visible near-infrared and shortwave-infrared (VNIR–SWIR: 380–2500 nm) and thermal-infrared (TIR: 6000–14 500 nm) spectral ranges with a spatial resolution of 8 mm (Hancock et al., 2013). Data are collected as raw spectra and line scan images of samples and are processed using 'The Spectral Geologist' software. The system is capable of detecting common rock-forming minerals (feldspar, quartz, pyroxene, garnet, olivine, carbonate, and phosphate), as well as a wide range of hydroxyl-bearing minerals.

Results

Stylolite mineralogy

The resolution of the HyLogger-3 is somewhat lower than the width of stylolites (1–5 mm), but quartz and ankerite were nevertheless detected in TIR spectra, and SWIR spectra show strong muscovite absorption and also the presence of minor Fe-chlorite. These results were validated using SEM/EDX analysis, which shows traces of Fe, Ca, Na, and Mg that indicate the presence of an illitic component in the sericite-rich (K and Al) host quartz vein. It also confirmed that gold coexists with Fe-chlorite (Fig. 6).

Gold and carbon do not have a spectral response in the current HyLogger wavelength range.

Paulsens

Gold from Paulsens was sampled from two different settings within the quartz vein host rock: a) visible gold associated with stylolites; and b) fine-grained gold spatially associated with massive sulfide. Variations in Ag content and the size and morphology of gold grains further suggest six distinct styles of gold — three in each of these settings (Table 2):

Gold associated with stylolites:

1. irregular fracture-fill gold in stylolitic quartz
2. interstitial gold in arsenopyrite crystals
3. spongy gold in pyrite within arsenopyrite.

Gold associated with massive sulfide:

4. isometric and drop-like gold in massive pyrrhotite
5. irregular gold grains in cavities within massive pyrrhotite
6. irregular gold grains within pyrrhotite that replaces massive pyrite.

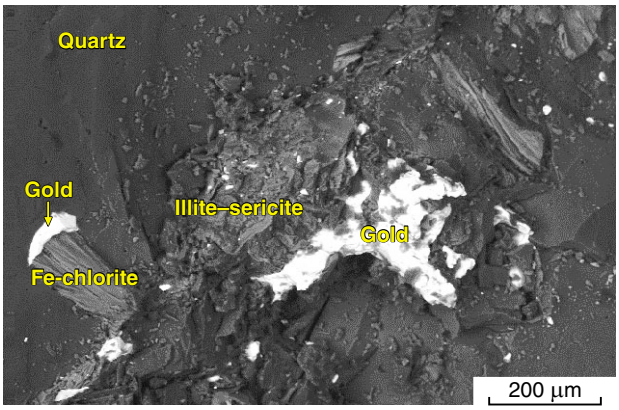

Figure 6. Back-scattered electron (BSE) image of a rough surface of a gold-bearing, stylolitic vein quartz from Paulsens. Gold (white) is associated with a seam of Fe-chlorite (fibrous) and sericite–illite in the vein quartz host rock (homogenous grey). Sample GSWA 201909

Assemblage 1: irregular fracture-fill gold in stylolitic quartz

Vein quartz from the Lower Zone at Paulsens (GSWA sample 201915) has a grey colour arising from the abundant and irregular stylolites, and associated fine-grained (<0.2 mm) gold. In contrast, vein quartz from the Upper Zone (GSWA samples 201909, 201910, 201911) is less stylolitic and more milky, with larger (0.1 – 10 mm) irregular particles of visible gold. Stylolitic material consists of graphitic illite–sericite–Fe-chlorite–ankerite–pyrite–arsenopyrite assemblage.

Gold displays a simple polycrystalline microstructure, with individual crystals ranging in size from 20–500 µm. Both polysynthetic and simple coherent twins are abundant (Fig. 7), and a few curved and deformed, incoherent twin planes were also observed (Fig. 8). Spot SEM/EDX analyses of gold show an Ag content of 6.8 – 7.6 wt% and only minor variation within each sample (Table 3). Of the 55 elements analysed by LA-ICP-MS, only Ag, Cu, and Hg are consistently present in the gold at concentration levels higher than background (Table 4). These elements show similar relative levels in all four gold samples. Sporadic enrichment in Fe, Pb, and Bi is also observed, especially in small grains. Antimony shows relatively high concentrations in large gold grains, but lower than threshold values in small grains due to swamping by contamination by other elements.

Table 2. Paulsens gold assemblages

	Paulsens gold assemblage	*Size µm*	*Shape*	*Ag wt%*	*Trace elements*	*GSWA sample no.*
1	Stylolitic quartz vein with graphitic illite–sericite–Fe-chlorite–ankerite–pyrite–arsenopyrite	>100	Irregular interstitial	6.8 – 7.6	Cu, Sb, Hg	201909 201910 201911 201915
2	Arsenopyrite crystals in stylolites	<500	Irregular intergranular	7.0	n/a	201909 201910
3	Pyrite grains relicts in stylolite-hosted arsenopyrite	<<20	Spongy irregular	n/a	n/a	201910
4	Massive pyrrhotite	10–600	Isometric drop-like	8.0 – 8.5	Cu, Sb, Hg, Fe, Co, Ni, Zn, Pb, Bi	201916
5	Massive pyrrhotite cavities with quartz and Fe oxides	10–100	Irregular	6.0	Cu, Sb, Hg	201916
6	Pyrrhotite replacing massive pyrite	10–200	Irregular angular	6.6 – 7.2	Cu, Sb, Hg, Fe, Co, Ni, Zn, Pb, Bi	201917

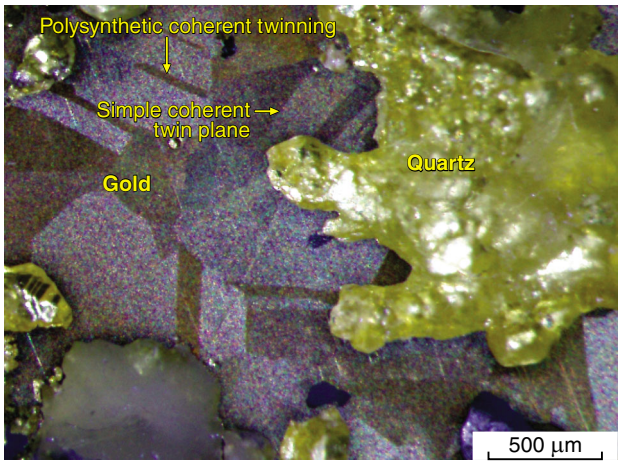

Figure 7. Reflected light photomicrograph of cut, polished, and etched stylolite-hosted gold from Paulsens. The gold (grey) in quartz (yellow) shows a simple polycrystalline microstructure together with examples of polysynthetic and simple coherent twinning. Sample GSWA 201910

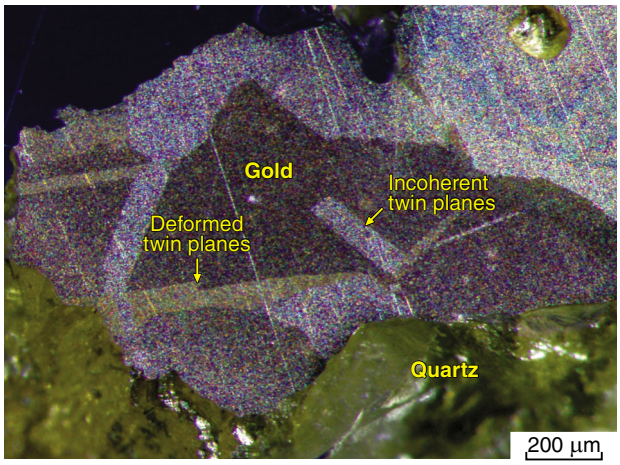

Figure 8. Reflected light photomicrograph of cut, polished, and etched stylolite-hosted gold from Paulsens. The gold (grey) in quartz (yellow) shows the development of curved and deformed incoherent twin planes. Sample GSWA 201909

Assemblage 2: interstitial gold in arsenopyrite crystals within stylolites

GSWA samples 201909 and 201910 are from relatively large (2 mm) sulfide segregations from the Upper Zone. Gold occurs as numerous small (<500 µm) irregular grains within arsenopyrite crystals (Fig. 9) and in intergranular spaces (Fig. 10). Small arsenopyrite crystals were also observed along stylolites from the Lower Zone; however, these did not contain visible gold inclusions. Gold grains have a twinned microstructure, with individual crystals less than 100 µm (Fig. 10). They contain 7 wt% Ag, but the small grain size precluded determination of their trace-element composition.

Assemblage 3: spongy gold in pyrite within arsenopyrite

GSWA sample 201910, obtained from the Upper Zone, has dust-like (≤20 µm), spongy-textured gold occurring in fine-grained pyrite that is preserved as relicts within a large, stylolite-hosted arsenopyrite crystal (Fig. 9). Microstructural and chemical analyses of this gold were not due to its very small grain size. A 300 µm gold grain was observed in association with a stylolite-hosted euhedral pyrite crystal in the same sample (Fig. 9), but this occurrence appears more similar to gold in Assemblage 2, and unrelated to the spongy-textured gold.

Table 3. Energy-dispersive X-ray data and number of analyses of Ag weight percentage in lode gold from Paulsens (GSWA 201909, 201910, 201911, 201915, 201916, and 201917) and placer gold from Mount Olympus (GSWA 201912, 201913, and 201914)

GSWA sample no.	*Ag wt %*		*n*
	min	*max*	
Paulsens			
201909	7.2	7.3	3
201910	7.0	7.0	1
201911	6.8	7.0	3
201915	7.1	7.6	4
201916	6.0 – 6.1 (3)	8.0 – 8.5 (7)	10
201917	6.6	7.2	5
Mount Olympus			
201912		7.0	2
201913	6.6	5.5	2
201914 (4 nuggets)	3.8 (2)	8.6 – 8.9 (2)	11
	5.5 (2)	9.7 – 9.9 (5)	

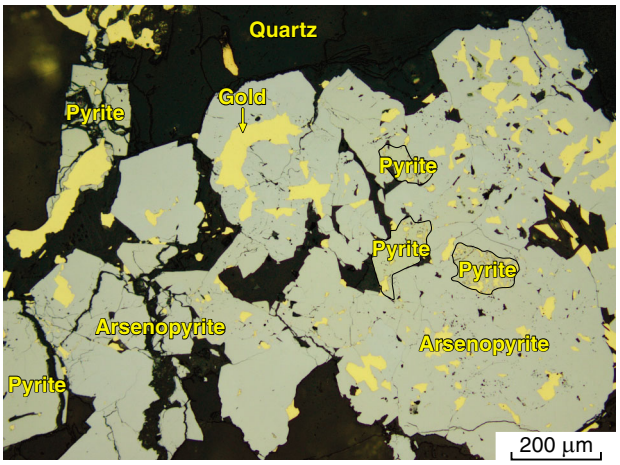

Figure 9. Reflected light photomicrograph of a cut and polished sample of gold from Paulsens. Gold (yellow) occurs in an arsenopyrite matrix (grey), together with grains of pyrite (Py, yellow-grey). Sample GSWA 201910

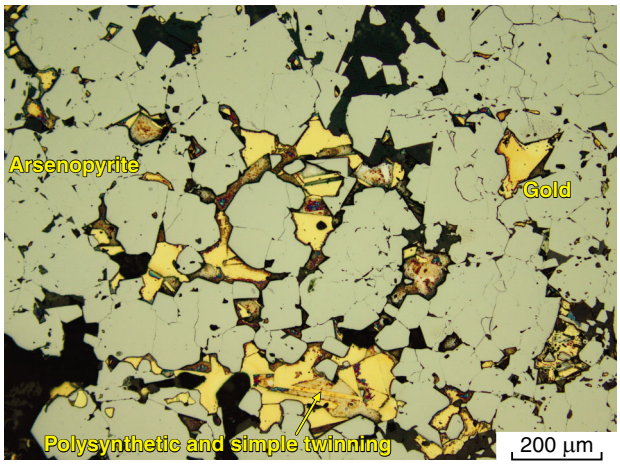

Figure 10. Reflected light photomicrograph of cut, polished, and etched sample of gold from Paulsens. Gold (yellow) occurs in intergranular space of arsenopyrite crystal (grey) and shows simple coherent and polysynthetic twinning. Sample GSWA 201909

Assemblage 4: isometric and drop-like gold in massive pyrrhotite

GSWA sample 201916 contains isometric and drop-like gold grains ranging in size from 10–600 µm in massive pyrrhotite (Fig. 11). Both morphologies show a simple monocrystalline twinned microstructure, and the gold typically contains 8.0 – 8.5 wt% Ag, consistently higher (by 1 – 1.5%) than for other Paulsens gold. The trace-element composition of three drop-like gold grains shows a general enrichment in Cu, Sb, and Hg, and an occasional enrichment in Fe, Co, and Ni, as well as Zn, Pb, and Bi.

Assemblage 5: irregularly shaped gold grains in massive pyrrhotite

GSWA sample 201916 also contains smaller (10–100 µm), irregular gold segregations associated with quartz and Fe oxides in small cavities within pyrrhotite (Fig. 12). The internal structure of gold grains appears to be monocrystalline, although this is often difficult to determine due to their limited response to acid etching. Silver content of the gold is relatively low (6 wt% Ag) and a single trace-element analysis shows high concentrations of Cu, Sb, and Hg, similar to other Paulsens gold.

Table 4. Laser ablation inductively coupled plasma mass spectroscopy data for lode gold from Paulsens (GSWA 201909, 201910, 201911, 201915, 201916, and 201917) and placer gold from Mount Olympus (GSWA 201912, 201913, and 201914)

GSWA sample no.	*Fe57*	*Co59*	*Ni60*	*Zn64*	*Cu65*	*As75*	*Ag109*	*Sb121*	*Hg202*	*Pb208*	*Bi209*
201909	<dl	<dl	91	<dl	1173220	<dl	460402368	6185	4162764	<dl	3117
201910	<dl	82	174	<dl	1569667	172	401254848	10276	3385655	71	<dl
201911	<dl	<dl	63	<dl	1417185	<dl	431014752	7422	3367710	<dl	<dl
201912	<dl	<dl	<dl	<dl	1396807	67	441374528	233	13837023	117	75
201913	355	<dl	<dl	<dl	855435	<dl	397967072	732	47808572	<dl	<dl
201914a	<dl	<dl	<dl	<dl	1714368	116	238773056	403	18844556	273	73
201914b	5463	219561	94906	<dl	612273	475202	508500480	1551	39818876	1671	105
201914c	<dl	67	71	94	1151906	<dl	551096192	475	46723760	834	51
201914d	<dl	<dl	<dl	<dl	388465	351	624520704	4963	14996658	325	154
201914e	<dl	<dl	94	90	403759	103	633320768	10850	16370674	414	462
201914f	<dl	<dl	122	<dl	1191479	<dl	323481792	698	5026765	94	<dl
201915a	57528	581	356	979	121371	<dl	79588941	776	7842495	1262	20146
201915b	7240	231	15	<dl	86950	207	54409949	234	5466688	383	17954
201915c	<dl	84	227	10	51379	<dl	68788349	363	4874854	371	6631
201916b	<dl	47	<dl	<dl	122270	<dl	92835995	98497	1971915	29	<dl
201916c	165	<dl	<dl	264	84270	11	90363061	10275	1676762	136	157
201916d	<dl	<dl	11	107	106099	<dl	82166360	68979	1981631	<dl	<dl
201916e	925149	5076	270762	10504	96761	133	100227458	1421883	2306140	913	7872
201917a	6041297	73947	45846	2720	117113	169	95833308	26620	2444879	1541	16756
201917b	104	<dl	<dl	<dl	173626	<dl	68465712	111559	1613319	39	55
201917c	27381	19	47	533	147479	59	82384431	26776	1777106	89	4064
201917d	<dl	<dl	64	<dl	154468	<dl	76922691	20273	2112358	131	778

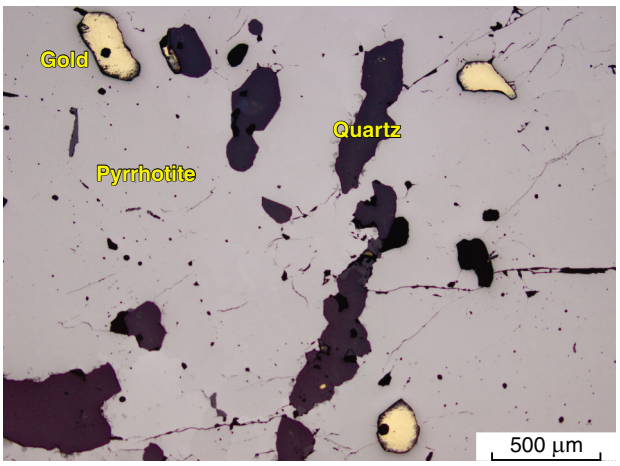

Figure 11. Reflected light photomicrograph of cut and polished sample GSWA 201916 showing rounded and drop-like shape of gold (yellow) and quartz (dark grey) in massive pyrrhotite matrix (grey)

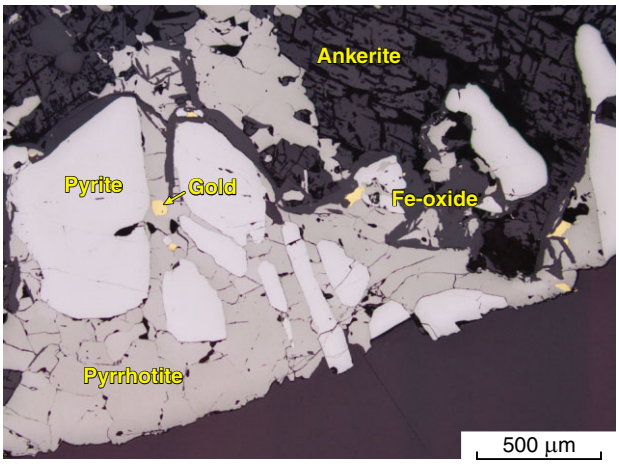

Figure 13. Reflected light photomicrograph of cut and polished sample GSWA 201917 showing pyrite (light grey) and gold grains (yellow) located in pyrrhotite (grey) and carbonate–Fe-oxides matrix (dark grey)

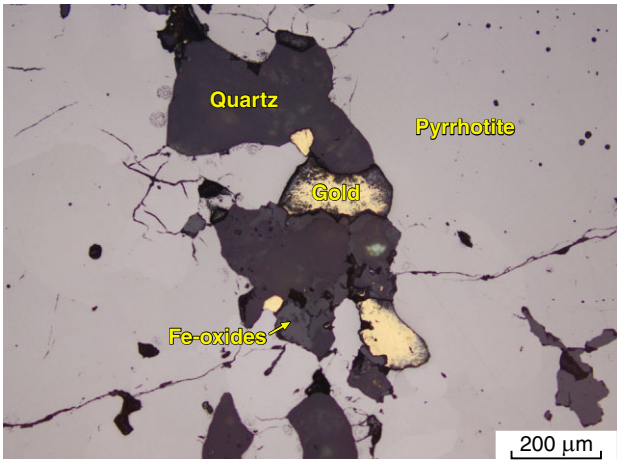

Figure 12. Reflected light photomicrograph of cut and polished sample GSWA 201916 showing irregular shape gold (yellow) with quartz–Fe-oxides (dark grey) within massive pyrrhotite matrix (grey)

Assemblage 6: irregular gold grains within pyrrhotite replacing massive pyrite

GSWA sample 201917 comprises intergrown quartz–carbonate–pyrite–pyrrhotite–chalcopyrite. Pyrrhotite has partly replaced pyrite grain margins and fills the intergranular spaces. All visible gold is within pyrrhotite, even where spatially associated with quartz and unaltered pyrite (Fig. 13). Gold grains range in size from 10–200 µm and are irregular to sporadically angular, with a simple monocrystalline microstructure and some twin planes. They contain 6.6 – 7.2 wt% Ag and high levels of Cu, Sb, and Hg. The very high Cu levels appear to be a primary characteristic, consistent with the spatial association of the gold with chalcopyrite. The elevated levels of Fe, Co, Ni, Zn, Pb and Bi evident in one analysis probably reflect contamination from the adjacent pyrrhotite.

Mount Olympus

Placer gold from Mount Olympus was derived from ferruginous quartz veins, and shows considerable variation in morphology, roundness, surface features, and the amount of quartz and Fe-oxide inclusions. GSWA sample 201912 comprises two specimens of native gold aggregates in Fe-rich fractures between quartz grains. All gold projecting outside the quartz is compressed and crumpled, and shows minor mechanical deformation, resulting from grain collision in the placer environment. GSWA sample 201913 is a rounded aggregate of porous Fe-oxide with spongy, platy, and lumpy gold. GSWA sample 201914 comprises four nuggets that range from well rounded, with smooth aggregates cemented by solid Fe-oxide (nuggets 1 and 2), to only slightly rounded, with irregular, pitted and spongy surfaces due to imprints from associated quartz grains (nuggets 3 and 4).

All Mount Olympus gold samples generally have a primary polycrystalline and twinned microstructure. Some grains are locally much more deformed and directionally orientated, with incoherent, broken, curved twin planes or translated zones (e.g. GSWA 201912; Fig. 14). Others, such as nuggets 1, 2, and 3 in GSWA sample 201914 exhibit less twinning; nugget 3 is only slightly rounded, and has a simple polycrystalline mosaic structure lacking twin planes (Fig. 15). Subgrains within each nugget vary in size from about 2 mm (GSWA 201914-1) to less than 100 µm (GSWA 201914-3). A more detailed SEM imaging of etched gold microstructures reveals in all gold

segregations the presence of thin, high-purity, intergranular veinlets that range in length from 10–100 µm and width up to 10 µm (Fig. 16). The surfaces of the gold grains also display triangular and rhomb-shape pits, reflecting the crystal lattice orientation of the gold (triangles lying parallel with the [111] crystallographic plane; Fig. 16). One grain's segregation displays a recrystallized corrosive rim up to 10 µm wide and partly recrystallized zones (Fig. 17). Another has a complex microstructure with several intergranular veinlets, banded around recrystallized crystals, and curved incoherent twin planes (Fig. 18).

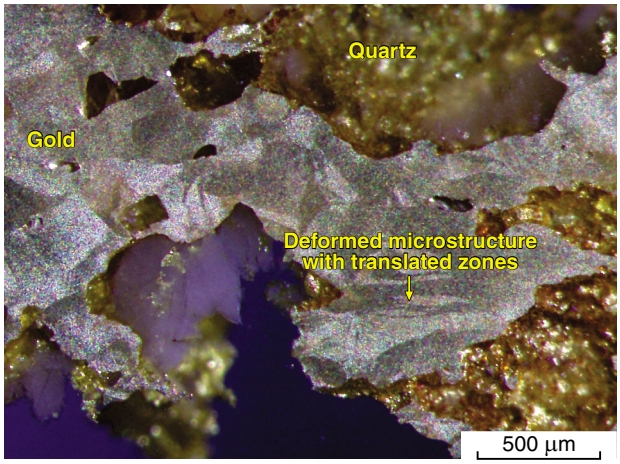

Figure 14. Reflected light photomicrograph of cut, polished, and etched placer gold from Mount Olympus. The gold (grey) in quartz (yellow) shows a deformed microstructure with directionally orientated translated zones. Sample GSWA 201912

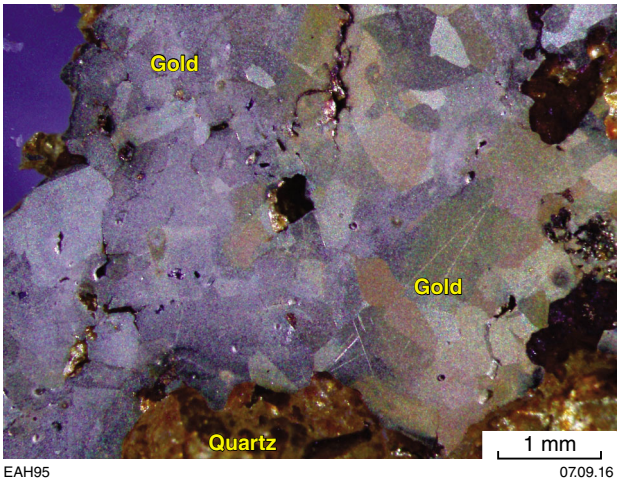

Figure 15. Reflected light photomicrograph of cut, polished, and etched placer gold from Mount Olympus. The gold (grey, pink) in quartz (yellow) shows a simple polycrystalline mosaic structure and a lack of twin planes. Sample GSWA 201914

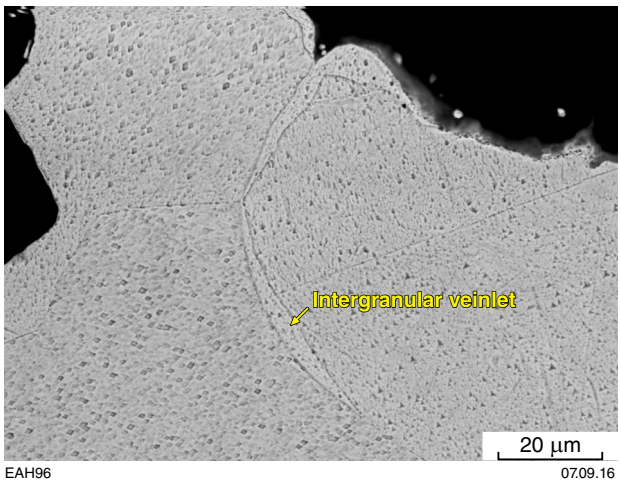

Figure 16. BSE image of a cut, polished, and etched sample of placer gold from Mount Olympus showing high-purity intergranular veinlets connecting to the edge of the grain through an embryonic corrosive rim. The triangular and rhomb-shape pitted surface of the grain (bottom right) reflects the crystal lattice orientation of the gold, with the triangles lying on the crystallographic plane parallel to the [111] plane. Sample GSWA 201912

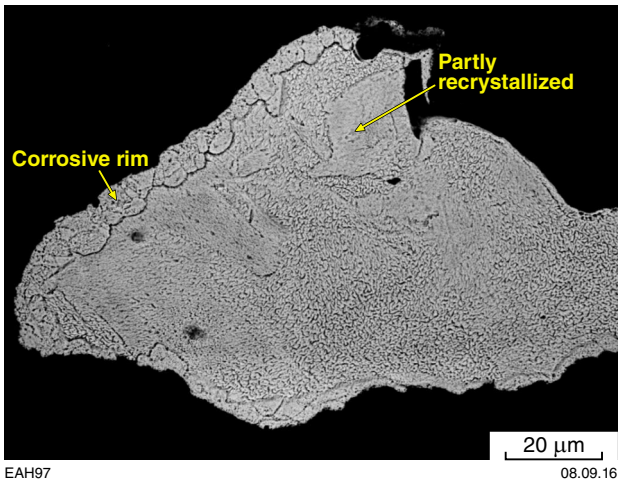

Figure 17. BSE image of a cut, polished, and etched sample of placer gold from Mount Olympus showing the development of a recrystallized corrosive rim around the margin of one crystal and partial grain recrystallization. Sample GSWA 201914

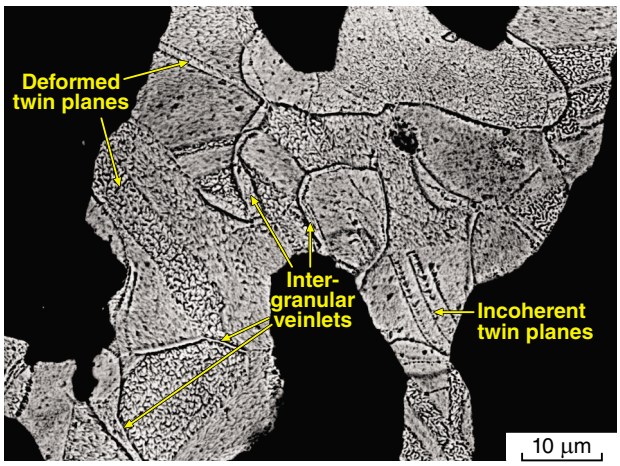

Figure 18. BSE image of a cut, polished, and etched sample of placer gold from Mount Olympus showing strongly deformed part of grain with the occurrence of several high-purity intergranular veinlets, banded around recrystallized crystals, and curved, incoherent twin planes. Sample GSWA 201914

Spot FE-SEM/EDX analysis of Mount Olympus placer gold reveals an Ag content ranging from <3.8 – 9.9 wt% (Table 3). Two gold nuggets (GSWA sample 201912 and GSWA sample 201914-4) show no silver in grain rims, but the interiors of these grains have silver contents up to 9.9 wt%.

The trace-element composition of gold in GSWA samples 201912, 201913 and 201914 were determined by LA-ICP-MS (Table 4). The ablation sites were carefully chosen to avoid any mineral inclusions, although one analysis (GSWA sample 201914b) did detect a Ni–Co-rich, submicroscopic arsenopyrite grain. All LA-ICP-MS results are similar to those from Paulsens, in that of the 55 elements analysed, only Ag, Cu, Sb, and Hg are present in relative concentration levels higher than background. In contrast to Paulsens gold, however, the relative concentrations of these elements are more variable, especially Sb, which shows two orders of magnitude difference in value between samples. In addition, all Mount Olympus samples have relatively high values of Hg.

Discussion

Physical and chemical conditions of gold deposition

This study is based on examination of only a small number of gold-bearing samples. Despite this, it is evident that the majority of lode gold samples from Paulsens (assemblages 1, 2, 5, and 6) and most of the colluvial placer gold from Mount Olympus have similar primary microstructures and chemistries that are consistent with precipitation from relatively low-temperature hydrothermal solutions under physically dynamic, but chemically stable, conditions. The simple primary monocrystalline or polycrystalline microstructure of gold from both locations indicates that it experienced at most only weak, low-pressure and low-temperature postdepositional alteration (although the primary features of gold from Mount Olympus have been modified by supergene processes). Polycrystallinity results from annealing/recrystallization of gold during deformation at elevated temperatures (Hough et al., 2007), which for gold with >5 wt% Ag requires a temperature greater than 250˚C (Butt and Timms, 2011). Abundant polysynthetic and simple coherent twins imply that gold precipitation was rapid and was accompanied by strong mechanical deformation (Petrovskaya, 1973; Smallman, 1990). Postdepositional deformation appears to be limited to sporadic development of random, curved, incoherent twinning and minor deformation of the grain boundaries (Nikolaeva et al., 2004; Hough et al., 2007). No samples show granoblastic recrystallization and disintegration of the primary microstructure, which indicates that the gold was not significantly affected by younger tectonothermal events. There is also no evidence of overprinting by another gold generation.

Enrichment of the gold in Cu, Sb, and Hg is a metallogenic signature typical of gold from low-grade metasedimentary rocks elsewhere in the Capricorn Orogen (Hancock et al., 2009). These elements are probably in solid solution within the gold lattice (Petrovskaya, 1973). Preservation of elevated levels of volatile elements such as Sb and Hg is also further evidence for lack of significant postdepositional alteration of the gold (though high Hg content in the Mount Olympus gold could be due to chemisorption from solutions in the supergene environment; Young et al., 2003; Nikolaeva et al., 2004). High Co and Ni concentrations (up to several hundred ppm based on a comparison with the known Ag concentration) in sulfide-hosted gold (assemblages 4 and 6) at Paulsens could have been inherited from the associated pyrite and/or pyrrhotite, in which the concentration of these elements may reach 0.1 wt% (Campbell and Ethier, 1984). Consistently higher Cu in gold from assemblage 6 can be explained by its spatial association with chalcopyrite.

The depositional setting is unclear for assemblages 3 and 4 at Paulsens. Thomas et al. (2011) suggested that Au (and As) can be released into solution when pyrrhotite replaces diagenetic Au-bearing and As-bearing pyrite during prograde metamorphism, then reprecipitated in the presence of organic matter. Gold remobilization by sulfide recrystallization during deformation at elevated temperatures is a mechanism interpreted for many mesothermal gold deposits in the Yilgarn Craton (Vaughan and Kyin, 2004). This process forms more coarsely grained sulfide crystals and releases and transports submicroscopic gold to be reprecipitated in a coarser free phase. It is possible that the spongy gold in relict pyrite in Paulsens assemblage 3 preserves an earlier mineralization event in which refractory gold was contained within the pyrite lattice. The (later) main mineralizing event that produced Paulsens assemblages 1, 2, 5, and 6 then partially remobilized, but did not fully recrystallize, this pyrite-hosted gold. In the Upper Zone this event was

responsible for the replacement of massive, Au-bearing and As-bearing pyrite with pyrrhotite, and also for the crystallization of arsenopyrite, pyrite, chalcopyrite, and free gold. In the massive, sulfide-poor Lower Zone, circulating hydrothermal solutions precipitated in stylolitic quartz more finely grained free gold that was sourced either from pyrite in the Upper Zone, or from elsewhere in the Paulsens system.

The occurrence of massive pyrite and pyrrhotite in the Upper Zone at Paulsens implies a relatively low-temperature hydrothermal mineralization event. However, the droplet-shaped morphologies and curvilinear boundaries in Paulsens assemblage 4 suggest that there may have been some partial melting of the sulfides. Partial melting of sulfide ores can occur at low temperatures (>281˚C) if low-melting-point chalcophile elements (such as bismuth) are present, and can then scavenge metals with high melting points such as gold and produce native metals (Fougerouse et al., 2016).

Provenance of Mount Olympus gold

The alluvial/colluvial gold nuggets obtained near the Mount Olympus deposit are quite dissimilar in character to mineralization at Mount Olympus, which is sediment-hosted, fine-grained, and spatially associated with arsenian pyrite (Young et al., 2003). The nuggets are derived from ferruginous quartz veins, display the primary polycrystalline microstructure, and have relatively high Ag and low As contents. The coarse grain size, slightly flattened shapes, paucity of marginal high-purity veinlets and corroded rims, and admixture with host rocks in the nuggets suggest that they have been transported only short distances from their primary sources, and have experienced only brief periods of immobility in the weathering environment; hence, they were derived from the immediate Mount Olympus region. This therefore implies a gold mineralizing event separate to that which created the main Mount Olympus deposit. The textural and chemical evidence is inconsistent with primary formation of the nuggetty gold by supergene enrichment of the main Mount Olympus deposit, but it is possible that a hydrothermal event recovered gold from pyrite at Mount Olympus and recrystallized it within quartz veins.

The Mount Olympus nuggets have been subjected to varying degrees of mechanical plastic deformation during transport in the supergene environment, resulting in gold grains with zones of directionally oriented crystals, bent twin planes, and small, patchily recrystallized grains and edge zones. Silver-depleted rims, thin, high-purity gold veinlets and small segregations, and a single corroded grain rim are probably expressions of weak supergene chemical alteration. The corroded rims probably developed at the electrolyte–alloy interface during periods of alluvium immobility, while ambient solutions had a pH of <5 (Nikolaeva et al., 2004; Hough et al., 2007).

Relative timing of gold mineralization

The microstructure and trace-element chemistry of gold used in our study provide little evidence for major postdepositional modification at Paulsens and Mount Olympus. Nevertheless, it is still possible to recognize three generations of gold, based upon variations in its grain size and shape, Ag and trace-element content, and the nature of the associated mineral assemblages:

1. Fine-grained, spongy-textured gold occurring in altered pyrite (Paulsens assemblage 3). This gold appears to be similar to the arsenian pyrite-hosted lode gold at Mount Olympus (Young et al., 2003); however, it appears to have been recrystallized to a coarser grained form.
2. Isometric and drop-like gold in massive Ni–Co-rich pyrrhotite (Paulsens assemblage 4). There may be an analogue to this event at Mount Olympus: one gold nugget has a submicroscopic inclusion of Ni–Co-rich arsenopyrite.
3. Gold in Paulsens assemblages 1, 2, 5, and 6 appears to be genetically related. It was precipitated from relatively low-temperature hydrothermal solutions: in (i) stylolitic quartz (assemblage 1); (ii) as irregular gold segregations in intergranular spaces within arsenopyrite (assemblage 2); (iii) by dissolution-reprecipitation of gold in fractures of massive pyrrhotite (assemblage 5); and (iv) in pyrrhotite–chalcopyrite replacing massive pyrite (assemblage 6). Similarities between Mount Olympus alluvial/colluvial gold and Paulsens assemblages 1, 2, 5, and 6 suggest that the Mount Olympus nuggets were derived from quartz veins that were possibly formed during the same hydrothermal event.

On the basis of available textural and chemical evidence, we infer the earliest (ore-forming) mineralization event at Paulsens (Generation 1) to be that which caused the partial recovery of refractory gold from pyrite. Generation 2 gold (represented by Paulsens assemblage 4) formed during a chalcophile-rich, relatively low-temperature hydrothermal partial melting episode, and may have been contemporaneous with Generation 1, although evidence for relative timing relationships is as yet lacking. The bulk of gold mineralization at Paulsens (represented by assemblages 1, 2, 5, and 6), and most of the Mount Olympus alluvial/colluvial gold, appears to have formed during the youngest, Generation 3 hydrothermal event.

Absolute timing of gold mineralization

Similarities in mineralogy and chemistry between much of the gold at Paulsens (assemblages 1, 2, 5, and 6) and in the Mount Olympus nuggets suggest that they may have formed during the same (Generation 3) hydrothermal event. The absolute age of this gold mineralizing event has not been determined, however, and must be inferred in the context of the interpreted geological history of the northern Capricorn Orogen.

Generation 3 gold shows little evidence for strong deformation and chemical modification, suggesting that it must have precipitated after both the 2215–2145 Ma Ophthalmian Orogeny and the early development of the Ashburton Fold Belt during the Capricorn Orogeny (1820–1776 Ma D_{1ash}/M_{1ash}; Thorne et al., 2011). Fine-grained sediment-hosted gold at Mount Olympus was deposited at c. 1738 Ma, after the M_{2ash} regional metamorphism but during D_{2ash} dextral strike-slip faulting in the Ashburton Fold Belt (Young et al., 2003, Sener et al., 2005). The D_{2ash} dextral strike-slip faulting was also responsible for major reactivation of the Nanjilgardy Fault along the southern margin of the exposed Pilbara Craton.

The lack of significant deformation in Generation 3 gold in Paulsens assemblages 1, 2, 5, and 6 and Mount Olympus gold nuggets suggests that they are younger than the main mineralization at Mount Olympus — perhaps related to the final stages of the 1776–1738 Ma D_{2ash} event, or even the more localized 1738–1620 Ma D_{3ash}/M_{3ash} event (Thorne et al., 2011). However, the gold could also have deposited during one of the many Paleoproterozoic to Neoproterozoic tectonic events recorded in the central Capricorn Orogen, the effects of which have not been widely reported from the northern margin. These include the 1680–1620 Ma Mangaroon Orogeny, the 1385–1170 Ma Mutherbukin Tectonic Event, the 1030–955 Ma Edmundian Orogeny, and the c. 570 Ma Mulka Tectonic Event (Sheppard et al., 2005, 2007, 2010; Johnson et al., 2011, 2013). Other major thermal events affecting the Capricorn Orogen might also be responsible, such as those associated with emplacement of the c. 1500 Ma Waldburg Dolerite, the c. 1465 Ma Narimbunna Dolerite, and the c. 1070 Ma Kulkatharra Dolerite (Wingate, 2002, 2012).

The absolute ages of the two older gold mineralizing events at Paulsens (represented by assemblages 3 and 4) are also unknown. They could have occurred at any time between deformation of the host stratigraphy and formation of the quartz vein (during the 2215–2145 Ma Ophthalmian Orogeny?) up to the time of formation of Generation 3 gold at Paulsens (assemblages 1,2, 5, and 6) and Mount Olympus (post c. 1738 Ma). The fine-grained, spongy-textured gold in altered pyrite at Paulsens (assemblage 3) is broadly similar to descriptions of arsenian pyrite-hosted lode gold at Mount Olympus and possibly could have formed during the same event at c. 1738 Ma.

Conclusions

This study investigates the mineralogy of lode and placer gold from the Paulsens and Mount Olympus deposits, in order to better understand the physical and chemical conditions during gold mineralization. Despite differences in host-rock geology, both the Paulsens and Mount Olympus deposits are located close to the Nanjilgardy Fault, a major, mantle-tapping structure, formed along the southern margin of the exposed Pilbara Craton.

Paulsens gold occurs in four styles: a) a very fine-grained phase spatially associated with massive pyrite; b) along stylolites, especially in the Lower Zone; c) a less common, coarse-grained phase in vein quartz; and d) spatially associated with massive pyrrhotite within the quartz vein host. Only visible gold associated with fractures and stylolites and fine-grained gold spatially associated with massive sulfide was examined during this study. It occurs in six assemblages:

1. Irregular fracture-fill gold in stylolitic quartz. Gold grains are >100 µm and have an Ag content of 6.8 – 7.6 wt% and elevated levels of Cu, Sb, and Hg. They display a simple polycrystalline microstructure.

2. Interstitial gold in arsenopyrite crystals. Gold grains are small (<500 µm) with a polycrystalline twinned microstructure and contain 7 wt% Ag.

3. Spongy-textured gold in pyrite within arsenopyrite. Gold is very fine-grained and dust like (≤20 µm).

4. Isometric and drop-like gold in massive pyrrhotite. Gold grains range in size from 10–600 µm and display a simple monocrystalline and polycrystalline twinned microstructure. They contain 8.0 – 8.5 wt% of Ag and show a general enrichment in Cu, Sb, and Hg and an occasional enrichment in Co, Ni, and Bi.

5. Irregular gold grains in cavities in massive pyrrhotite. Gold grains are small (10–100 µm) and contain 6 wt% Ag, together with high concentrations of Cu, Sb, and Hg. The internal structure of gold grains appears to be monocrystalline.

6. Irregular gold grains within pyrrhotite replacing massive pyrite. Gold grains range in size from 10–200 µm and shapes are irregular and sometimes angular. They contain 6.6 – 7.2 wt% Ag and high levels of Cu, Sb, and Hg with occasional enrichment in Co, Ni, and Bi. The gold has a simple monocrystalline microstructure with some twin planes.

Placer gold nuggets from Mount Olympus were derived from ferruginous quartz veins, located 2–3 km from the main c. 1738 Ma sediment-hosted mineralization. The placer gold shows significant variation in its morphology and the amount of quartz and Fe-oxide inclusions. All gold has a primary polycrystalline and twinned microstructure, with only minor deformed incoherent, broken and curved twin planes and translated zones. Thin, high-purity intergranular veinlets are abundant. Placer gold has an Ag content ranging from < 3.8 – 9.9 wt%. Using LA-ICP-MS analysis only four elements (Ag, Cu, Sb, and Hg) are present in concentration levels higher than background. The relative content of these elements, especially Sb, is variable, and all samples have high values of Hg.

Most of the Paulsens gold (assemblages 1, 2, 5, and 6) and quartz vein-sourced placer gold from Mount Olympus show similarities in their primary microstructure and chemistry that indicate both were precipitated from low-temperature hydrothermal solutions under physically

dynamic, but chemically stable conditions. Gold from both sources has experienced only weak, low-pressure and low-temperature postdepositional alteration, although in the case of the placer gold the primary features have been modified in response to supergene processes. The depositional setting for the sulfide-hosted gold at Paulsens (assemblages 3 and 4) is uncertain but appears to have occurred during an earlier, relatively low-temperature hydrothermal melting event or events.

Our study indicates that most of the gold mineralization at Paulsens (assemblages 1, 2, 5, and 6) and in Mount Olympus vein quartz post-dates both the 2215–2145 Ma Ophthalmian Orogeny and the 1820–1776 Ma Capricorn Orogeny. It may have occurred during the final stages of c. 1738 Ma dextral strike-slip faulting in the southern Pilbara, but it could also have formed during one of the many Paleoproterozoic to Neoproterozoic tectonic events recorded in the central Capricorn Orogen. The ages of the two older gold mineralizing events at Paulsens (assemblages 3 and 4) are unknown and could have occurred at any time between the initial deformation of the host stratigraphy (Ophthalmian Orogeny?) and the formation of Paulsens assemblages 1, 2, 5, and 6.

Acknowledgements

The authors gratefully acknowledge Northern Star Resources staff and especially Philip Tornatora and Imogen Fielding for their support of this study and donation of gold-bearing samples, and Imogen's contribution to enhance the publication. We thank Michael Verrall for his help with the FE-SEM/EDX operation and Derek Winchester for the preparation of gold sections at CSIRO, Kensington, Western Australia. We are particularly grateful to Philip and Debbie Wilson for providing us with the placer gold from the Mount Olympus area.

References

Butt, CRM and Timms, NE 2011, The Liversidge nugget collection: a new look at some old gold: Australian Journal of Earth Sciences 58, p. 777–791.

Campbell, FA and Ethier, VG 1984, Nickel and cobalt in pyrrhotite and pyrite from the Faro and Sullivan orebodies: Canadian Mineralogist, v. 22, p. 503–506.

Fougerouse, D, Micklethwaite, S, Tomkins, AG, Mei, Y, Kilburn, M, Guagliardo, P, Fisher, LA, Halfpenny, A, Gee, M, Paterson, D and Howard, DL, 2016 Gold remobilisation and formation of high grade ore shoots driven by dissolution-reprecipitation replacement and Ni substitution into auriferous arsenopyrite: Geochimica et Cosmochimica Acta, v. 178, p. 143–159.

Hancock, EA, Thorne, AM, Morris, PA, Watling, RJ and Cutten, HNC 2009, Mineralogy and trace element chemistry of lode and alluvial gold from the western Capricorn Orogen: Geological Survey of Western Australia, Record 2009/6, 30p.

Hancock, EA and Thorne, AM 2011, Mineralogy of lode and alluvial gold from the western Capricorn Orogen, Western Australia: Australian Journal of Earth Sciences 58, p. 793–801.

Hancock, EA, Green, AA, Huntington, JK, Schodlok, MC and Whitbourn, LB 2013, HyLogger-3: implications of adding thermal-infrared sensing: Geological Survey of Western Australia, Record 2013/3, 24p.

Hough, RM, Butt, CRM, Reddy, SM and Verrall, M 2007, Gold nuggets: supergene or hypogene?: Australian Journal of Earth Sciences, v. 54, p. 959–964.

Johnson, SP, Sheppard, S, Thorne, AM, Rasmussen, B, Fletcher, IR, Wingate, MTD and Cutten, HN 2011, The role of the 1280–1250 Ma Mutherbukin Tectonic Event in shaping the crustal architecture and mineralization history of the Capricorn Orogen, *in* GSWA 2011 extended abstracts: promoting the prospectivity of Western Australia: Geological Survey of Western Australia, Record 2011/2, p. 1–3.

Johnson, SP, Thorne, AM, Tyler, IM, Korsch, RJ, Kennett, BLN, Cutten, HN, Goodwin, J, Blay, OA, Blewett, RS, Joly, A, Dentith, MC, Aitken, ARA, Holzschuh, J, Salmon, M, Reading, A, Heinson, G, Boren, G, Ross, J, Costelloe, RD and Fomin, T 2013, Crustal architecture of the Capricorn Orogen, Western Australia and associated metallogeny: Australian Journal of Earth Sciences, v. 60, no. 6–7, p. 681–705, doi:10.1080/08120099.2013.826735.

Krapeẑ, B, Müller, SG and, Bekker, A 2015, Stratigraphy of the Late Palaeoproterozoic (~2.03 Ga) Wooly Dolomite, Ashburton Province, Western Australia: A carbonate platform developed in a failed rift basin: Precambrian Research, v. 271, p. 1–19.

Nikolaeva, LA, Gavrilov, AM, Nekrasova, AN, Yablokova, SV and Shatilova, LV 2004, Native gold in lode and placer deposits of Russia, *in* Atlas: Central Research Institute of Geological Prospecting for Base and Precious Metals (TsNIGRI), Moscow, 176p.

Northern Star Resources Ltd 2012, Paulsens–Geology and mineralisation, AIG-MEGWA presentation, September 2012, viewed 27 November 2014: http://www.aig.org.au/images/stories/Resources/nst_aig_presentation_sept2012_20120919.pdf.

Petrovskaya, NV 1973, Native Gold: Nauka, Moscow, Russia, 347p.

Rasmussen, B, Fletcher, IR and Sheppard, S 2005, Isotopic dating of the migration of a low-grade metamorphic front during orogenesis: Geology, v. 33, p. 773–776.

Sener, AK, Young, C, Groves, DI, Krapez, B and Fletcher, IR 2005, Major orogenic episode associated with Cordilleran-style tectonics related to the assembly of Paleoproterozoic Australia?: Geology, v. 33, p. 225–228.

Sheppard, S, Occhipinti, SA and Nelson, DR 2005, Intracontinental reworking in the Capricorn Orogen, Western Australia: the 1680–1620 Ma Mangaroon Orogeny: Australian Journal of Earth Sciences, v. 52, p. 443–460.

Sheppard, S, Rasmussen, B, Muhling, JR, Farrell, TR and Fletcher, IR 2007, Grenvillian-aged orogenesis in the Palaeoproterozoic Gascoyne Complex, Western Australia: 1030–950 Ma reworking of the Proterozoic Capricorn Orogen: Journal of Metamorphic Geology, v. 25, p. 477–494.

Sheppard, S, Johnson, SP, Wingate, MTD, Kirkland, CL and Pirajno, F 2010, Explanatory Notes for the Gascoyne Province: Geological Survey of Western Australia, Perth, Western Australia, 336p.

Smallman, RE 1990, Modern Physical Metallurgy: Butterworths, London, 530p.

Thomas, HV, Large, RR, Bull, SW, Maslennikov, V, Berry, RF, Fraser, R, Froud, S and Moye, R 2011, Pyrite and pyrrhotite textures and composition in sediments, laminated quartz veins, and reefs at Bendigo gold mine, Australia: Insights for ore genesis: Economic Geology, v. 106, no. 1, p. 1–31.

Thorne, AM, Johnson, SP, Tyler, IM, Brett, JW, Cutten, HN, Blay, O, Korsch, RJ, Kennett, BLN, Blewett, RS, Joly, A, Dentith, MC, Holzschuh, J, Goodwin, J, Salmon, M, Reading, A and Boren, G 2011, Preliminary interpretation of deep seismic reflection line 10GA–CP1: crustal architecture of the northern Capricorn Orogen, *in* Capricorn Orogen seismic and magnetotelluric (MT) workshop 2011: extended abstracts *edited by* SP Johnson, AM Thorne, and IM Tyler: Geological Survey of Western Australia, Record 2011/25, p. 19–26.

Thorne, AM 2016a, Wyloo Group (P_-WY-s): Geological Survey of Western Australia, WA Geology Online, Explanatory Notes extract, viewed 07 June 2016, <www.dmp.wa.gov.au/ens>.

Thorne, AM 2016b, Shingle Creek Group (P_-SK-xb-s): Geological Survey of Western Australia, WA Geology Online, Explanatory Notes extract, viewed 07 June 2016, <www.dmp.wa.gov.au/ens>.

Young, CJ, Groves, DI and Morant, P 2003, Sediment-hosted disseminated gold mineralisation in the Paleoproterozoic Ashburton Province, Western Australia: a new epizonal orogenic gold province related to Capricorn Orogeny? *in* Mineral Exploration and Sustainable Development: proceedings of the 7th Biennial SGA Meeting, Athens, Greece.

Vaughan, JP and Kyin, A 2004, Refractory gold ores in Archaean greenstones, Western Australia: mineralogy, gold paragenesis, metallurgical characterization and classification: Mineralogical Magazine, v. 68, no. 2, p. 255–277.

Watling, RJ, Herbert, HK, Delev, D and Abell, ID 1994, Gold fingerprinting by laser ablation inductively coupled plasma mass spectrometry: Spectrochimica Acta, v. 49B, no. 2, p. 205–219.

Wingate, MTD 2002, Age and palaeomagnetism of dolerite sills of the Bangemall Supergroup on the Edmund 1:250 000 sheet, Western Australia: Geological Survey of Western Australia, Record 2002/4, 48p.

Wingate, MTD, Kirkland, CL, Cutten, HN and Thorne, AM 2012, 143445: dolerite sill, Waldburg Homestead; Geochronology Record 1077: Geological Survey of Western Australia, 4p.

RECORD 2016/14

MINERALOGY OF GOLD FROM THE PAULSENS AND MOUNT OLYMPUS DEPOSITS, NORTHERN CAPRICORN OROGEN, WESTERN AUSTRALIA

Hancock and Thorne

This Record is published in digital format (PDF) and is available as a free download from the DMP website at <www.dmp.wa.gov.au/GSWApublications>.

Further details of geological products produced by the Geological Survey of Western Australia can be obtained by contacting:

Information Centre
Department of Mines and Petroleum
100 Plain Street
EAST PERTH WESTERN AUSTRALIA 6004
Phone: +61 8 9222 3459 Fax: +61 8 9222 3444
www.dmp.wa.gov.au/GSWApublications